Cisplatin (*cis*-$Pt(NH_3)_2Cl_2$) and *cis*-$[Pt(NH_3)_2(H_2O)_2]^{2+}$ Intrastrand Cross-Linking Reactions at the Telomere GGGT DNA Sequence Embedded in a Duplex, a Hairpin, and a Bulged Duplex: Use of Mg^{2+} and Zn^{2+} to Convert a Hairpin to a Bulged Duplex

Julie M. Villanueva,[†] Xin Jia,[†] Paulos G. Yohannes,[‡] Paul W. Doetsch,[‡,§] and Luigi G. Marzilli*[,†]

Departments of Chemistry and Biochemistry, Emory University, Atlanta, Georgia 30322, and Division of Cancer Biology and Department of Radiation Oncology, Emory University School of Medicine, Atlanta, Georgia 30322

Received May 25, 1999

In the past, we showed that metal species have a high affinity for the central G in the GGG sequence of the duplex $d(A_1T_2G_3G_4G_5T_6A_7C_8C_9C_{10}A_{11}T_{12})_2$ (**G3-D**) and that cisplatin (*cis*-$Pt(NH_3)_2Cl_2$) and **G3-D** formed an N7−Pt−N7 G_4,G_5 intrastrand cross-link preferentially over the G_3,G_4 adduct (∼25:1). Thus, a putative G_4 monoadduct was postulated to cross-link in the 3′- rather than the normally more favorable 5′-direction. To evaluate this hypothesis and also to explore why the **G3-D** G_4,G_5 adduct had an unusual hairpin structure, we have now introduced the use of *N*,*N*′-dimethylthiourea (DMTU) as a monoadduct trap and have extended the study to a **G3-D** analogue with a hairpin form, $d(A_1T_2G_3G_4G_5T_6T_7C_8C_9C_{10}A_{11}T_{12})$ (**G3-H**). Chemical shift and 2D ^1H and ^{13}C NMR data indicated that the **G3-H** hairpin has a stem region with B-form structure and a nonhelical loop region. Zn^{2+} or Mg^{2+} ions transformed **G3-H** into a bulged duplex. Downfield shifts of G_4H8 and G_4C8 NMR signals indicated that Zn^{2+} binds preferentially to G_4N7. Reaction of cisplatin or *cis*-$[Pt(NH_3)_2(H_2O)_2]^{2+}$ with the bulged duplex and hairpin forms of **G3-H** gave a similar intrastrand cross-link ratio, G_4,G_5:G_3,G_4 = 7:3. This ratio is insensitive to DNA form or Pt leaving group. For **G3-D** this ratio is lower in the *cis*-$[Pt(NH_3)_2(H_2O)_2]^{2+}$ reaction (∼1:1) than in the cisplatin reaction (25:1), indicating that the leaving group influences the cross-linking step for **G3-D**. The G_4 monoadducts of the *cis*-$Pt(NH_3)_2Cl_2$−**G3-H** and −**G3-D** and the *cis*-$[Pt(NH_3)_2(H_2O)_2]^{2+}$−**G3-D** reactions were trapped with DMTU, but no monoadduct was trapped in the *cis*-$[Pt(NH_3)_2(H_2O)_2]^{2+}$−**G3-H** reaction. The results suggest that the respective monoadducts are more long-lived for **G3-D**. We postulate that the G_5 in the **G3-D** Cl-G_4 monoadduct is placed in a favorable position to form the cross-link because of a prior conformational change induced by G_4−A_7 stacking. This accounts for the very high selectivity for 3′-cross-linking. Nevertheless, in all other cases, regardless of the form or conformation, 3′-direction cross-linking is unusually favored at GGGT sequences, suggesting that the sequence itself contributes greatly to the 3′-cross-linking preference; since telomeres have multiple repeats of this GGGT sequence, this finding may have biological relevance.

Introduction

Non-B-form shapes of DNA such as cruciform, hairpin, and quadruplex forms are essential for important biological functions. Since nucleic acids are quite malleable, DNA conformation can be manipulated by metal binding. Telomeres, repeats found at the end of chromosomes to promote genetic stability,[1−3] can exist in various conformations.[4−6] The G-rich sequence of telomeres, which extends beyond the C-rich strand in human telomeres ∼130−210 base pairs,[4,5] has been shown to form G-quadruplexes which are stabilized by M^+ (K^+, Na^+) coordinating to the guanine O6's.[6,7] Toxic metal ions such as Hg(II) can change the form of DNA, converting hairpins to duplexes.[8] Although hairpin forms of DNA have been shown to be important in regulating biological processes such as replication, transcription, and translation,[9−17] there have been

* Corresponding author.
[†] Department of Chemistry, Emory University.
[‡] Department of Biochemistry, Emory University.
[§] Division of Cancer Biology and Department of Radiation Oncology, Emory University School of Medicine.

(1) Bodnar, A. G.; Ouellette, M.; Frolkis, M.; Holt, S. E.; Chiu, C.-P.; Morin, G. B.; Harley, C. B.; Shay, J. W.; Lichtsteiner, S.; Wright, W. E. *Science* **1998**, *279*, 349−352.
(2) Counter, C. M. *Mutat. Res.* **1996**, *366*, 45−63.
(3) Ishikawa, F. *Biochem. Biophys. Res. Commun.* **1997**, *230*, 1−6.
(4) Henderson, E. R.; Blackburn, E. H. *Mol. Cell. Biol.* **1989**, *9*, 345−348.
(5) Makarov, V. L.; Hirose, Y.; Langmore, J. P. *Cell* **1997**, *88*, 657−666.
(6) Fletcher, T. M.; Sun, D.; Salazar, M.; Hurley, L. H. *Biochemistry* **1998**, *37*, 5536−5541.
(7) Marathias, V. M.; Bolton, P. H. *Biochemistry* **1999**, *38*, 4355−4364.
(8) Kuklenyik, Z.; Marzilli, L. G. *Inorg. Chem.* **1996**, *35*, 5654−5662.
(9) Ausubel, F. M.; Brent, R.; Kingston, R.; Moore, D. D.; Seidman, J. G.; Smith, J. A.; Struhl, K. In *Current Protocols in Molecular Biology*; Wiley-Interscience: New York, 1991; Vol. I.
(10) Benight, A. S.; Wang, Y.; Amaratunga, M.; Chattopadhyaya, R.; Henderson, J.; Hanlon, S.; Ikuta, S. *Biochemistry* **1989**, *28*, 3323−3332.
(11) Blommers, M. J. J.; Walters, J. A. L. I.; Haasnoot, C. A. G.; Aelen, J. M. A.; van der Marel, G. A.; van Boom, J. H.; Hilbers, C. W. *Biochemistry* **1989**, *28*, 7491−7498.
(12) Persson, C.; Wagner, E. G. H.; Nordstrom, K. *EMBO J.* **1990**, *9*, 3767−3775.
(13) Waga, S.; Mizuno, S.; Yoshida, M. *J. Biol. Chem.* **1990**, *265*, 19424−19428.

10.1021/ic990603f CCC: $18.00
Published on Web 12/09/1999

only a few studies of the effects of metal ions on DNA hairpin structure and properties.[18,19]

Metal species greatly affect the shape and properties of DNA in vitro, but the study of such effects in vivo is difficult because of the lability of most metal species and the fluxional character and numerous binding sites of DNA.[20] The best example showing a relationship between structural changes induced by metal binding to DNA and an important set of biological consequences is found in the mechanism of action of the clinically important anticancer drug cisplatin (*cis*-$Pt(NH_3)_2Cl_2$).[21−29] This drug forms inert DNA adducts and distorts DNA structure. Several proteins that recognize non-B-form DNA structures other than duplexes bind well to cisplatin−DNA adducts. High mobility group (HMG) proteins, which bind to kinks and bends in DNA,[21] also bind to cisplatin lesions, perhaps shielding the platinated site from repair[22−24] and/or inhibiting translesion synthesis.[25] The mismatch repair protein hMSH2, responsible for the repair of base−base mismatches and small loops,[27] also binds to cisplatin adducts.[28] hMSH2 is overexpressed in testicular and ovarian tissues, suggesting that hMSH2 binding to cisplatin−DNA adducts may be important in the anticancer activity.[28] DNA distortions caused by cisplatin adducts require detailed investigation because these distortions should affect protein binding and subsequent anticancer activity.

In the past, we found that the oligomer $d(A_1T_2G_3G_4G_5T_6A_7C_8C_9C_{10}A_{11}T_{12})$ (**G3-D**) is a good model for evaluating the structural response of DNA to both labile metal ions and to cisplatin in solution.[30] Although **G3-D** is a duplex at 12 °C, a hairpin form was found at higher temperatures at low concentrations of oligonucleotide and salt. Addition of Zn^{2+} eliminated the hairpin form. We now report studies on $d(A_1T_2G_3G_4G_5T_6T_7C_8C_9C_{10}A_{11}T_{12})$ (**G3-H**) with A_7 of **G3-D** replaced with T_7. The central TT mismatches destabilize the duplex form and thus favor the hairpin form. The GGGTT sequence in **G3-H** is found in the multiply repeated human telomere sequence.[31−34] The GGGTT sequence is a potentially excellent target for reaction with cisplatin. Shortening and degradation of telomeres has been shown in cisplatin-treated HeLa cells.[35] Previously we reported that the binding of cisplatin and $Pt(en)Cl_2$ (en = ethylenediamine) to **G3-D** was highly selective: the G_4,G_5 intrastrand cross-linked product greatly predominated over G_3,G_4 and G_3,G_5 adducts (Scheme 1).[36,37] The results suggested that cisplatin attacked at G_4 and cross-linked to G_5 (3′-cross-linking or 3′-chelation, Scheme 2). Ordinarily, 5′-cross-linking is preferred.

Scheme 1

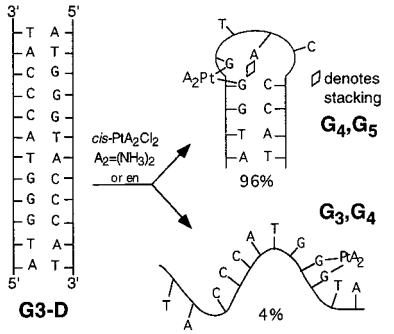

Scheme 2

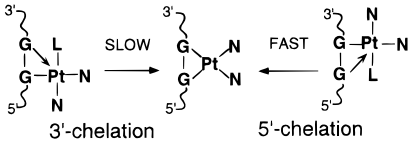

The present investigation of **G3-D** and **G3-H** was undertaken to assess the effect of structural variation on the reaction of the three-G sequence with cisplatin. To gain further insight into metal control of DNA structure, we have studied by NMR spectroscopy the structural transitions of **G3-H** caused by Zn^{2+} and Mg^{2+}. Zn^{2+} is known to interact with unprotonated nucleobase nitrogens and with the backbone phosphate groups, whereas Mg^{2+} exhibits only the latter interaction. We examined the effect of metal binding and consequential structural distortions of DNA on the reaction of **G3-H** and **G3-D** with *cis*-$Pt(NH_3)_2Cl_2$ and *cis*-$[Pt(NH_3)_2(H_2O)_2]^{2+}$. With electrophoretic techniques,[37] cross-linked products of **G3-H** and **G3-D** are easily resolved and quantitated to determine product ratios and platination sites. The use of *N*,*N*′-dimethylthiourea (DMTU) to trap various monoadducts was also investigated to determine the initial binding site, information needed to assess the preferred cross-linking direction. Finally we showed previously that the G_4,G_5 cross-link stabilized an irregular hairpin structure of **G3-D**.[36] In this **G3-D** structure, A_7 was tucked inside the hairpin loop and stacked above G_4. The stacking interaction between A_7 and G_4 stabilized the irregular hairpin form (Scheme 1).[36] In the analogous **G3-H** adduct, T_7 replaces A_7. Thymine base stacking is normally weaker than adenine base stacking, and we expected the hairpin form to be less stable.

Experimental Section

Materials. **G3-H** and **G3-D** were synthesized by the phosphoramidite method[38] and purified as described by Kline.[39] All other materials were obtained from commercial sources. Oligonucleotide concentrations

(14) Spiro, C.; Richards, J. P.; Chandrasekaran, S.; Brennan, R. G.; McMurray, C. T. *Proc. Natl. Acad. Sci. U.S.A.* **1993**, *90*, 4606−4610.
(15) Higashitani, A.; Greenstein, D.; Hirokawa, H.; Asano, S.; Horiuchi, K. *J. Mol. Biol.* **1994**, *237*, 388−400.
(16) Philippe, C.; Benard, L.; Portier, C.; Westhof, E.; Ehresmann, B.; Ehresmann, C. *Nucleic Acids Res.* **1995**, *23*, 18−28.
(17) Wilson, K. S.; von Hippel, P. H. *Proc. Natl. Acad. Sci. U.S.A.* **1995**, *92*, 8793−8797.
(18) Xu, Y.-C.; Bremer, H. *Nucleic Acids Res.* **1997**, *25*, 4067−4071.
(19) Young, K. J.; Gill, F.; Grasby, J. A. *Nucleic Acids Res.* **1997**, *25*, 3760−3766.
(20) Jia, X.; Marzilli, L. G. *Biopolymers* **1991**, *31*, 23−44.
(21) Bianchi, M. E.; Beltrame, M.; Paonessa, G. *Science* **1989**, *243*, 1056−1059.
(22) Pil, P. M.; Lippard, S. J. *Science* **1992**, *256*, 234−237.
(23) McA'Nulty, M. M.; Lippard, S. J. *Mutat. Res.* **1996**, *362*, 75−86.
(24) Dunham, S. U.; Lippard, S. J. *Biochemistry* **1997**, *36*, 11428−11436.
(25) Hoffmann, J.-S.; Locker, D.; Villani, G.; Leng, M. *J. Mol. Biol.* **1997**, *270*, 539−543.
(26) Treiber, D. K.; Zhai, X.; Jantzen, H.-M.; Essigmann, J. M. *Proc. Natl. Acad. Sci. U.S.A.* **1994**, *91*, 5672−5676.
(27) Kirkpatrick, D. T.; Petes, T. D. *Nature* **1997**, *387*, 929−931.
(28) Mello, J. A.; Acharya, S.; Fishel, R.; Essigmann, J. M. *Chem. Biol.* **1996**, *3*, 579−589.
(29) Drummond, J. T.; Anthoney, A.; Brown, R.; Modrich, P. *J. Biol. Chem.* **1996**, *271*, 19645−19648.
(30) Jia, X.; Zon, G.; Marzilli, L. G. *Inorg. Chem.* **1991**, *30*, 228−239.
(31) Moyzis, R. K.; Buckingham, J. M.; Cram, L. S.; Dani, M.; Deaven, L. L.; Jones, M. D.; Meyne, J.; Ratliff, R. L.; Wu, J.-R. *Proc. Natl. Acad. Sci. U.S.A.* **1988**, *85*, 6622−6626.
(32) Meyne, J.; Ratliff, R. L.; Moyzis, R. K. *Proc. Natl. Acad. Sci. U.S.A.* **1989**, *86*, 7049−7053.
(33) Nugent, C. I.; Hughes, T. R.; Lue, N. F.; Lundblad, V. *Science* **1996**, *274*, 249−252.
(34) Lin, J.; Zakian, V. *Proc. Natl. Acad. Sci. U.S.A.* **1996**, *93*, 13760−13765.
(35) Ishibashi, T.; Lippard, S. J. *Proc. Natl. Acad. Sci. U.S.A.* **1998**, *95*, 4219−4223.
(36) Iwamoto, M.; Mukundan, S.; Marzilli, L. G. *J. Am. Chem. Soc.* **1994**, *116*, 6238−6244.
(37) Yohannes, P. G.; Zon, G.; Doetsch, P. W.; Marzilli, L. G. *J. Am. Chem. Soc.* **1993**, *115*, 5105−5110.
(38) Stec, W. J.; Zon, G.; Egan, W.; Byrd, R. A.; Phillips, L. R.; Gallo, K. A. *J. Org. Chem.* **1985**, *50*, 3908−3913.
(39) Kline, T. P. Ph.D. Dissertation Thesis, Emory University, 1988.

in bases were determined by UV spectroscopy (ϵ_{260} at 95 °C = 7680 M^{-1} cm^{-1} per base for **G3-H** and ϵ_{260} at 25 °C = 6300 M^{-1} cm^{-1} per base for **G3-D**).[8,37] M^{2+}−oligomer samples were prepared with $ZnCl_2$ (for NMR experiments), $Zn(NO_3)_2$, or $Mg(NO_3)_2$ stock solutions and adjusting the pH to 6.0. The Zn^{2+} stock solution was prepared by weighing an appropriate amount of $ZnCl_2$ into a 50 mL volumetric flask and adding 2 drops of 5.5 M HCl and deionized water. The solution concentration, 0.1 M, was determined by atomic absorption spectroscopy. Other stock solutions were prepared similarly, using HNO_3 instead of HCl (no acid was added to the Mg^{2+} solution). Samples were lyophilized and then dissolved in 99.96% D_2O (0.5 mL), and the solution was transferred (under nitrogen) to a 5-mm NMR tube.

NMR Methods. ^{1}H and ^{13}C NMR Spectroscopy. Experiments were performed on a GE GN-500 spectrometer. 2D NMR experiments were performed at 12 °C, except where noted. Proton spectra (16K) were recorded typically with 5000 Hz sweep width, 30° pulse width, and a presaturation pulse for D_2O samples or 8000 Hz sweep width, 80° pulse width, and 1331 solvent suppression sequence for 90% H_2O/10% D_2O samples. For the saturation transfer and the NOE difference spectra, 16 and 128 scans, respectively, were collected with the saturating field directed off-resonance subtracted from an equal number of scans with the saturating field on-resonance. The chemical shift calibration was based on the signal of residual HOD. Homonuclear *J*-correlation spectroscopy (COSY)[8,40,41] (16 scans per t_1) and phase-sensitive 2D cross-relaxation correlation (NOESY)[42−44] (48 scans per t_1, 300 ms mixing time) with presaturation and ^{31}P decoupling utilized a 512 × 2048 data matrix size and a sweep width of 5000 Hz.

Heteronuclear multiple quantum correlation (HMQC)[45,46] spectral parameters included a 128 × 1024 data matrix size, 512 scans, 1.0 s, 5000 Hz sweep width for the ^{1}H dimension, 8065 Hz sweep width for the ^{13}C dimension (frequency = 125.76 MHz), 41 W of ^{13}C rf power, and a 38-μs 90° pulse width. Allowance was made for foldover. The FID's were apodized with sine square multiplication and zero-filled prior to the last Fourier transformation. The offset in the carbon dimension was calculated as described previously.[30] Similar acquisitions and processing parameters were used for heteronuclear multiple bond correlation (HMBC)[47] spectra, which were collected using a 128 × 512 data matrix size with 1024 scans per t_1.

^{31}P NMR Spectroscopy. ^{1}H-decoupled 16K ^{31}P NMR spectra with trimethyl phosphate (TMP) as reference were recorded at 146.134 MHz with a Nicolet 360-NB spectrometer (1400 Hz sweep width, 60° pulse width, 500 ms delay, and ∼20 000 scans).

Gel Electrophoresis. Polyacrylamide gel electrophoresis was performed according to a published procedure,[9] with gels prepared as previously described.[37] Denaturing and nondenaturing gel electrophoresis was carried out at room temperature and at 4 °C, respectively. Cross-linked product ratios for nonlabeled DNA were determined by analysis of scanned UV-shadowed gels using the Image Quant program.

***cis*-$Pt(NH_3)_2X_2$ Reactions with Oligonucleotides.** In a typical reaction using the method described,[39] an aqueous solution of the oligonucleotide (1−2 mM in strands) was mixed with 1 equiv/strand of *cis*-$Pt(NH_3)_2Cl_2$ in the presence or absence of various concentrations of $Mg(NO_3)_2$ or $Zn(NO_3)_2$. Solutions were kept at 4 °C in the dark for 4−5 days to ensure complete platination[37] and then stored at −20 °C. For *cis*-$[Pt(NH_3)_2(H_2O)_2]^{2+}$ reactions, an aqueous solution of *cis*-$Pt(NH_3)_2Cl_2$ was treated with $AgNO_3$ (2 equiv) for 1 day at 4 °C. AgCl was filtered from the *cis*-$[Pt(NH_3)_2(H_2O)_2]^{2+}$ solution before it was added to the oligonucleotides.

5′-End-Labeling Reactions. Platinated and unplatinated oligomers were 5′-end-labeled as previously described.[37] The reaction products were separated by electrophoresis on 20% nondenaturing or denaturing gels, visualized by autoradiography, and quantitated by liquid scintillation.

Modified Maxam−Gilbert Sequencing Reactions. Platinum binding sites were determined using base-specific chemical reactions on 5′-^{32}P-labeled oligos. Maxam−Gilbert G + A and C + T sequencing reactions[48] were performed. For the T-specific reaction, $KMnO_4$ (1 μL of a 5 mM solution) was added to an aqueous solution (8 μL) of 5′-end-labeled DNA, and after 5 min at room temperature, the reaction was quenched with allyl alcohol (1 μL).[49] The G-specific reaction with dimethyl sulfate (DMS) was performed for various times (1−10 min) as described.[48] The purine-specific reaction was performed with diethyl pyrocarbonate (DEPC) as described.[37] Products of the base-specific reactions were ethanol precipitated and lyophilized. (Platinated products were further treated with 0.1 M NaCN (50 μL, pH 7.0) at 37 °C for 20−40 h and reprecipitated.) All products were treated with 2 M piperidine at 90 °C for 30 min and lyophilized. After addition of deionized water (20 μL) and lyophilizing, the products were separated on 20% denaturing gels and analyzed by autoradiography.

Results

The ^{1}H NMR spectra of **G3-H** at 22 °C (Supporting Information) have four and six T methyl signals at low (∼45 mM) and high (∼90 mM) concentrations, respectively. Evidently, two interconverting forms of the oligomer are present at high concentration. Saturation transfer experiments indicated that the small peaks at 1.87 and 1.64 ppm exchanged with an overlapped peak at 1.61 ppm, and the small peaks at 1.53 and 1.43 ppm exchanged with an overlapped peak at 1.46 ppm. On the basis of previous studies,[50] such a concentration dependence between interconverting forms suggests that these are a hairpin form and a duplex form with a central bulged TT mismatch/loop. With dilution, the hairpin form is favored. To study the hairpin form, 2D NMR experiments were performed using a 45 mM solution (4 mM in strands).

Nonexchangeable Proton Assignments. The strategy for assigning the ^{1}H NMR CH signals was described earlier.[30,51−53] All signals except H5′/5″ were assigned with NOESY and COSY methods at 12 °C (Table 1, Figures 1 and 2, and Supporting Information). For comparison, the shifts of **G3-D** studied earlier[30] in the absence and presence of Zn^{2+} are also given. Spectra of **G3-H** were usually obtained at 12 °C since this temperature was used for the metal binding studies. Spectra obtained at 25 °C were better resolved, and the data confirmed the 12 °C assignments. Furthermore, the hairpin form of the oligomer is more favored at 25 °C than at 12 °C, and the spectrum lacks cross-peaks from the hairpin form (Figure 2).

Free G3-H. The most significant shift differences between **G3-H** and **G3-D** signals (Table 1) involved the middle of the strand, G_5 to C_9; e.g., the T_6H6 signal at 7.24 ppm for **G3-D** vs 7.64 ppm for **G3-H**. In comparison to the duplex, downfield shifts for G_5H8 and C_8H6 of **G3-H** were observed. Only the G_3N(1)H and the CH5 and CH6 shifts of the signals were similar for the hairpin and the duplex forms. The H1′ signals of T_6 to C_{10} were somewhat downfield compared to **G3-D**.

(40) Aue, W. P.; Bartholdi, E.; Ernst, R. R. *J. Chem. Phys.* **1976**, *64*, 2229−2242.
(41) Bax, A.; Freeman, R. *J. Magn. Reson.* **1981**, *4*, 542−561.
(42) Jeener, J.; Meier, B. H.; Bachmann, P.; Ernst, R. R. *J. Chem. Phys.* **1979**, *71*, 4546−4553.
(43) Kumar, A.; Ernst, R. R.; Wuthrich, K. *Biochem. Biophys. Res. Commun.* **1980**, *95*, 1−6.
(44) States, D. J.; Haberkorn, R. A.; Ruben, D. J. *J. Magn. Reson.* **1982**, *48*, 286−292.
(45) Muller, L. *J. Am. Chem. Soc.* **1979**, *101*, 4481−4484.
(46) Bax, A.; Subramanian, S. *J. Magn. Reson.* **1986**, *67*, 565−569.
(47) Bax, A.; Summers, M. F. *J. Am. Chem. Soc.* **1986**, *108*, 2093−2094.
(48) Maxam, A. H.; Gilbert, W. In *Methods in Enzymology*; Grossman, L., Moldave, K., Eds.; Academic Press: New York, 1980; Vol. 65; pp 499−650.
(49) Williamson, J. R.; Celander, D. W. *Nucleic Acids Res.* **1990**, *18*, 379.
(50) Summers, M. R.; Byrd, R. A.; Gallo, K. A.; Samson, C. J.; Zon, G.; Egan, W. *Nucleic Acids Res.* **1985**, *13*, 6375−6386.
(51) Hosur, R. V.; Ravi, K. M.; Roy, K. B.; Tan, Z.; Miles, H. T.; Govil, G. In *Magnetic Resonance in Biology and Medicine*; McGraw-Hill: New Delhi, 1985; pp 243−260.
(52) Hare, D. R.; Wimmer, D. L.; Cohn, S. H.; Drobny, G.; Reid, B. R. *J. Mol. Biol.* **1983**, *171*, 319−336.
(53) Scheek, R. M.; Russo, N.; Boelens, R.; Kaptein, R.; van Boom, J. H. *J. Am. Chem. Soc.* **1983**, *105*, 2914−2916.

Table 1. ^{1}H NMR Chemical Shifts (ppm) of Oligomers in the Absence and Presence of M^{2+} [a]

	G3-H			G3-D	
protons	no M^{2+}	Zn^{2+}	Mg^{2+}	no M^{2+}	Zn^{2+}
A_1H8	8.20	8.19	8.14	8.18	8.20
A_1H2	8.04	7.96	7.92	8.01	7.97
A_{11}H8	8.39	8.38	8.39	8.33	8.34
A_{11}H2	7.98	7.90	7.92	7.88	7.83
T_2H6	7.38	7.34	7.31	7.33	7.39
T_2CH_3	1.48	1.36	1.33	1.40	1.33
G_3H8	7.86	7.85	7.90	7.83	7.88
G_4H8	7.64	7.84	7.70	7.67	7.87
G_5H8	7.80	7.53	7.51	7.54	7.57
T_6H6	7.64	7.44	7.52	7.24	7.32
T_6CH_3	1.85	1.65	1.73	1.33	1.37
T_7H6	7.43	7.57	7.50		
T_7CH_3	1.42	1.51	1.53		
C_8H6	7.71	7.72	7.70	7.29	7.31
C_8H5	6.02	5.74	5.72	5.22	5.22
C_9H6	7.67	7.63	7.64	7.45	7.46
C_9H5	5.84	5.60	5.72	5.42	5.44
C_{10}H6	7.55	7.47	7.47	7.47	7.47
C_{10}H5	5.75	5.62	5.62	5.62	5.59
T_{12}H6	7.34	7.28	7.26	7.29	7.28
$T_{12}CH_3$	1.61	1.55	1.52	1.55	1.53

[a] Experimental conditions: 99.96% D_2O, pH 6.0 (uncorrected in D_2O), and 12 °C.

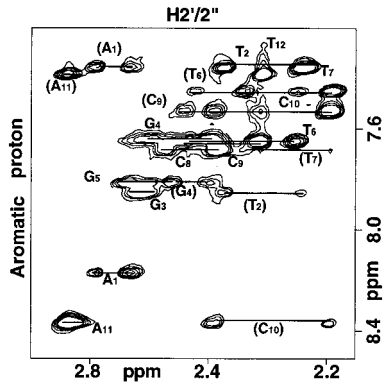

Figure 1. Contour plot of aromatic to H2′/2″ region of the NOESY spectrum of **G3-H** (45 mM in bases, 25 °C, D_2O). The intranucleotide H2′/2″ NOE cross-peaks are linked and labeled by the base number only. The internucleotide H2′/2″ cross-peaks to the aromatic proton signals in the 5′ direction are linked and labeled by the 5′-base number in parentheses.

A_1H8−T_2CH_3, C_9H6−C_{10}H5 and A_{11}H8−$T_{12}CH_3$ NOE cross-peaks (Figure 2 and Supporting Information) suggest that the stem region of **G3-H** is a right-handed helix with base stacking.[53] However, in the alternating purine-pyrimidine region, many interresidue NOE connectivities (e.g., A_1H1′−T_2H6, T_2-H1′−G_3H8, and C_{10}H1′−A_{11}H8) were very weak (Supporting Information). Strong cytosine intrabase H6−H5 NOE cross-peaks were also evident. Weaker NOE cross-peaks, typical of B-form duplex stems, included C_9H6−C_{10}H5, C_9H5−C_{10}H6, and T_7H6−C_8H5. It is notable that the C_8H6−C_9H5 NOE cross-peak, expected for a B-form duplex, was missing.

From G_4 to C_9, the overlapping NOE cross-peaks in the aromatic to H1′ region made sequential assignments difficult. However, unambiguous assignments were made on the basis of this region and other regions in the NOESY and COSY spectra as well as the HMQC spectrum. For example, the base proton signals (except for AH2's and A_1H8) have NOE cross-peaks to the 5′ H2′/2″ signals as well as to the intranucleotide H2′/2″ signals (Figure 1). The intranucleotide H8/H6−H2′/2″ NOE cross-peaks of G_3, G_5, and C_8 were severely overlapped

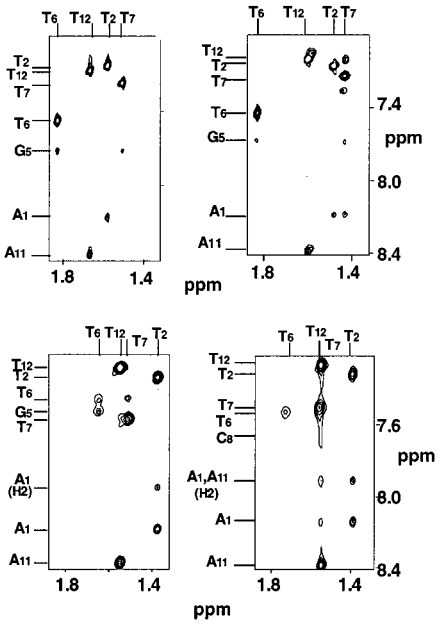

Figure 2. Contour plots of NOESY spectra (aromatic to T methyl region): free **G3-H** (45 mM in bases, in D_2O) at 25 °C (top left); free **G3-H** at 12 °C (top right); **ZnG3-H** bulged duplex at 12 °C (bottom left); **MgG3-H** bulged duplex at 12 °C (bottom right). Some assignments are indicated. The additional NOE cross-peaks in the top right plot are from the duplex form.

due to the similarity of the G_4H8, T_6H6, and C_9H6 chemical shifts. Fortunately, the H1′ to H2′/2″ region in the NOESY spectrum (Supporting Information) has no overlapping signals, and the H1′ signals of G_4, T_6, and C_9 are well resolved.

In the aromatic to the T methyl proton region of NOESY spectra for **G3-H** at 12 °C (Figure 2), there was no T_6H6−T_7CH_3 NOE cross-peak. This observation, together with the missing C_8H6−C_9H5 and very weak T_7H6−C_8H5 and T_6H1′−T_7H6 NOE cross-peaks, is consistent with an unstacked, nonhelical structure in the loop region. The G_5H8−T_6CH_3 NOE cross-peak suggests that these bases are stacked. However, there were no NOE connectivities from T_7CH_3 to C_8H6 and, in the other regions, from T_7H2′ to C_8H6 or C_8H5, although there was a very weak T_7H1′−C_8H6 NOE cross-peak. These observations suggest that the base T_7 is above G_5 inside the loop, whereas T_6 is relatively outside the loop.

Bulged G3-H Duplex with 6 Zn^{2+}. With Zn^{2+} addition, the number of ^{1}H NMR signals of **G3-H** at 22 °C nearly doubled at lower Zn^{2+} concentrations (2 or 3 Zn^{2+}/duplex) ratios but then, at higher Zn^{2+} concentrations (5 or 6 Zn^{2+}/duplex), decreased to approximately the same number as in the **G3-H** spectrum. Seen most clearly in the aromatic (Supporting Information) and T methyl proton spectral regions, these spectral changes suggest that a bulged duplex is formed. Upon addition of Zn^{2+}, the G_4H8 signal of the **G3-H** hairpin shifted from 7.64 to 7.75 ppm, indicating that Zn^{2+} binds to G_4N7 of the **G3-H** hairpin form. During the Zn^{2+} titrations, no differences were found between 5 Zn^{2+}/bulged duplex or 6 Zn^{2+}/bulged duplex. Thus, we refer to these bulged duplex species as **ZnG3-H**.

From the NOESY spectrum, complete assignments of the **ZnG3-H** signals were obtained (Table 1 and Supporting Information). In the aromatic and T methyl regions, Zn^{2+} induced large downfield shifts for the G_4H8, T_7H6, and T_7CH_3 signals. Large upfield shifts were seen for the G_5H8, T_6H6, T_6CH_3, and T_2CH_3 signals. The A_1H2, A_{11}H2, and C_{10}H6 signals also exhibited ∼0.08 ppm upfield shifts. Some H2′/2″ signals shifted either upfield or downfield, usually changing the shift

Table 2. Protonated ^{13}C NMR Chemical Shifts (ppm) of the Oligomers in the Absence and Presence of M^{2+} [a]

	G3-H[b]			G3-D[c]	
carbons	no M^{2+}	Zn^{2+}	Mg^{2+}	no M^{2+}	Zn^{2+}
A_1C8	142.8	142.4	141.7	142.4	142.5
A_1C2	154.6	154.4	154.1	154.5	154.5
T_2C6	139.0	139.1	138.6	138.7	139.0
T_2C_M	14.8	14.1	14.6	14.0	14.2
G_3C8	138.6	138.5	138.4	138.1	139.6
G_4C8	137.6	139.3	137.6	137.1	139.6
G_5C8	*d*	137.0	137.1	136.9	137.3
T_6C6	139.3	139.1	139.2	138.0	138.5
T_6C_M	14.9	14.8	15.5	14.3	14.1
T_7C6	139.3	139.9	138.7		
T_7C_M	15.1	14.5	15.1		
C_8C6	144.7	143.4	142.9	141.7	142.2
C_8C5	99.2	98.7	98.5	98.1	98.0
C_9C6	143.6	143.0	142.9	142.4	143.1
C_9C5	99.5	98.6	98.6	98.3	98.2
$C_{10}C6$	143.4	143.2	142.7	142.9	143.1
$C_{10}C5$	99.2	98.6	98.6	98.8	98.7
$A_{11}C8$	142.2	141.9	142.2	141.7	142.0
$A_{11}C2$	154.9	154.8	154.8	155.0	154.7
$T_{12}C6$	139.5	139.2	138.9	138.9	139.0
$T_{12}C_M$	15.0	14.4	14.9	14.2	14.3

[a] Experimental conditions: 99.96% D_2O and pH 6.0 (uncorrected in D_2O). [b] 25 °C. [c] 12 °C. [d] Resolved signal not observed.

difference between a given pair of H2′/2″ signals. The G_3H2″, G_4H2′,H2″, T_7H2′,H2″, C_8H2′,H2″, and C_9H2′ signals had the largest shifts.

Many of the NMR shifts of **ZnG3-H** were similar to those of **G3-D** with 8 Zn^{2+}/duplex (**ZnG3-D**). Exceptions included the shifts of aromatic and T methyl signals for the center of the strand, T_6, C_8, and C_9. These similarities and differences are consistent with formation of a bulged duplex by **G3-H**. From the significant downfield shift of the G_4H8 after adding Zn^{2+}, the favored position of Zn^{2+} binding to **G3-H** is likely to be G_4N7, as was found for **G3-D**.[30]

Strong or relatively strong A_1H8−T_2CH_3, A_{11}H8−$T_{12}CH_3$ (Figure 2), and C_8H6−C_9H5 NOE cross-peaks suggest a normal right-handed helix in the nonbulged termini of **ZnG3-H**. Strong G_5H8−T_6CH_3 NOE cross-peaks suggest G_5/T_6 base stacking. The fact that some NOE cross-peaks normally observed (G_5H8−G_4H2′,H2″ and T_6H6−G_5H2′,H2″) were not seen suggests that G_5 is not in a normal helix position. Weak T_6H6−T_7CH_3 (Figure 2), G_5H1′−T_6CH_3, and T_6H1′−T_7CH_3 NOE cross-peaks were also found. These facts together suggest that the bases in the bulged region are poorly stacked. It is noteworthy that the shifts of T_6CH_3 (1.65 ppm) and T_7CH_3 (1.51 ppm) in **ZnG3-H** differ; the greater shielding for T_7 suggests that T_7 is closer to the inside of the bulge than is T_6.

Bulged G3-H Duplex with 10 Mg^{2+}. The similar ^1H NMR shifts observed at 10 Mg^{2+}/bulged duplex (**MgG3-H**) and for **ZnG3-H**, especially for the middle of the strand from G_5 to C_{10}, indicate that **MgG3-H** is a bulged duplex. The G_4H8 shift is more upfield in **MgG3-H**, consistent with Zn^{2+} binding to N7 of G_4 in **ZnG3-H**. Relatively strong NOE cross-peaks were found for both flanking regions in **MgG3-H**, suggesting a well-developed helical structure with base stacking. The upfield shift of T_7CH_3 (1.53 ppm) vs T_6CH_3 (1.73 ppm) suggests that the T_7 base is inside the bulge and that the T_6 base is more exposed to solvent.

^{13}C NMR Assignments. Signals of protonated carbons of free **G3-H** as well as **ZnG3-H** and **MgG3-H** at 25 °C were assigned by HMQC methods (Table 2 and Supporting Information). The signals broadened upon addition of Zn^{2+} or Mg^{2+}.

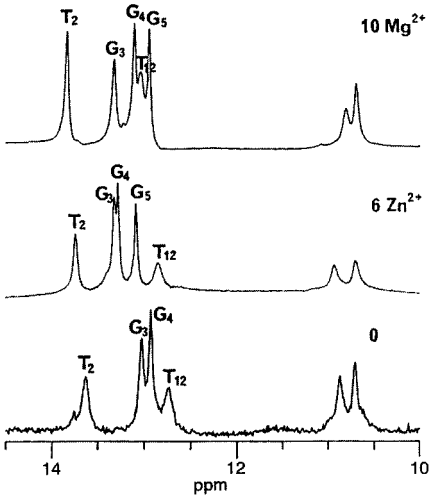

Figure 3. Imino proton NMR spectra of **G3-H** (45 mM) in the absence and presence of divalent metal cations at 12 °C in 90% H_2O/10% D_2O, pH 6.0. Assignments and the metal ion ratios (per bulged duplex) are indicated.

Nevertheless, assignments were possible by using the strategy based on the ^1H NMR assignments, as described earlier.[54−56] Most of the nonprotonated carbon signals were assigned from the HMBC experiment with free **G3-H** (Supporting Information). Although attempts were made to assign signals of nonprotonated carbons of **ZnG3-H** and **MgG3-H**, only A_1, T_2, A_{11}, and T_{12} signals were observed clearly, and these were not significantly different from those of free **G3-H** (data not shown).

Nearly all of the large shift differences from normal duplex values found (Table 2) are for signals corresponding to the central region of the oligomers. Upfield shifts occurred in the conversion from the hairpin to the bulged duplex form. For example, the normal duplex shift for T_6C1′ was ∼85−86 ppm, but the hairpin value was 88.3 ppm. When M^{2+} induced bulged duplex formation, a normal duplex shift was found. Furthermore, differences in the stem region of the hairpin suggest that the structure also differs somewhat from that in the duplexes.

Imino Proton Assignments. For **G3-H** in 90% H_2O/10% D_2O at 12 °C, the six imino proton signals observed (Figure 3) were assigned by the 1D NOE method. There was no NOE between the T_2N(3)H and T_{12}N(3)H signals, probably due to end fraying. The two upfield broad signals, which were not assigned, are for T_6N(3)H and T_7N(3)H. No signal for G_5N(1)H was observed for **G3-H**. However, for **ZnG3-H** seven peaks were seen at 12 °C (Figure 4). The signal for G_5N(1)H was assigned by 1D NOE spectroscopy. The signals downfield of 12.6 ppm shifted downfield after Zn^{2+} addition (Figure 3). Irradiation of the broad signal at 12.82 ppm produced an NOE to the A_1H2 signal, and the signal was assigned to T_{12}N(3)H. There was no NOE between the T_2N(3)H and T_{12}N(3)H signals, as also found without Zn^{2+}. The two upfield signals, T_6N(3)H and T_7N(3)H, broadened slightly with Zn^{2+} addition. The spectrum of **MgG3-H** at 12 °C also had seven peaks (Figure 5). Compared to **ZnG3-H**, the G_4N(1)H and G_5N(1)H signals were clearly more upfield. However, the T_2N(3)H and T_{12}N(3)H signals were more downfield, and all TN(3)H signals were sharper, especially the most upfield signal.

(54) Ashcroft, J.; LaPlante, S. R.; Borer, P. N.; Cowburn, D. *J. Am. Chem. Soc.* **1989**, *111*, 363−365.
(55) Leupin, W.; Wagner, G.; Nenny, W. A.; Wuthrich, K. *Nucleic Acids Res.* **1987**, *15*, 267−275.
(56) LaPlante, S. R.; Ashcroft, J.; Cowburn, D.; Levy, G. C.; Borer, P. N. *J. Biomol. Struct. Dyn.* **1988**, *5*, 1089−1099.

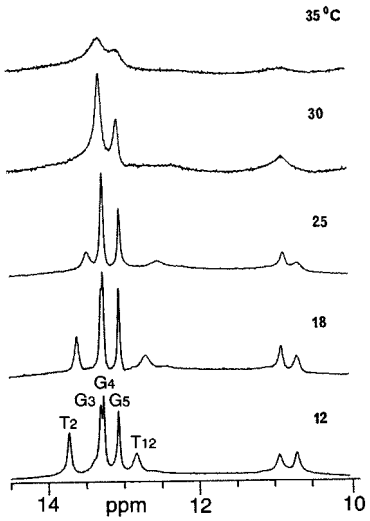

Figure 4. Imino proton NMR spectra of the **ZnG3-H** bulged duplex (45 mM in bases) in 90% H_2O/10% D_2O, pH 6.0, at various temperatures as indicated.

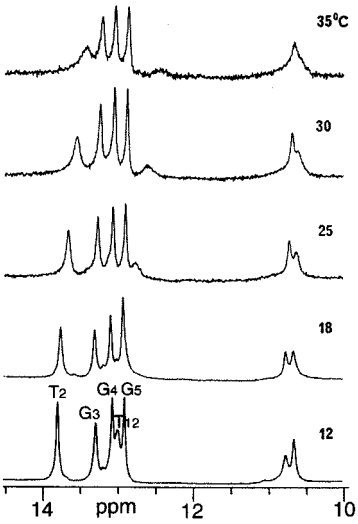

Figure 5. Imino proton NMR spectra of the **MgG3-H** bulged duplex (45 mM in bases) in 90% H_2O/10% D_2O, pH 6.0, at various temperatures as indicated.

For **ZnG3-H**, the T_2N(3)H and T_{12}N(3)H signals shifted upfield and broadened above 12 °C (Figure 4) and disappeared at 30 °C. The three GN(1)H signals broadened simultaneously but did not shift. These signals were no longer observed above 45 °C. The upfield imino signals for the bulged T's did not shift but broadened and disappeared. The most upfield signal at 10.7 ppm broadened at a higher temperature (35−40 °C) and is tentatively assigned to T_7N(3)H, which we believe is less exposed to solvent. Broadening and disappearance of imino signals occurred at similar temperatures with Zn^{2+} as without M^{2+} (Supporting Information), suggesting that the **G3-H** hairpin and **ZnG3-H** duplex have similar stabilities toward melting.

Although such preferential broadening was also observed for **MgG3-H** (Figure 5), two important differences were apparent: the upfield signals were very sharp at 12 °C, and the differences in chemical shifts were smaller. However, the upfield signal of **MgG3-H** broadened at ∼10 °C higher than that for **ZnG3-H**. Likewise, the broadening and upfield shifting of T_2N(3)H and T_{12}N(3)H signals occurred at ∼10 °C higher temperature. The GN(1)H signals did not shift upfield prior to their disappearance. The observation that higher temperatures were required in order for the imino signals of **MgG3-H** to disappear suggests that **MgG3-H** is more stable toward melting than **ZnG3-H** or free **G3-H**.

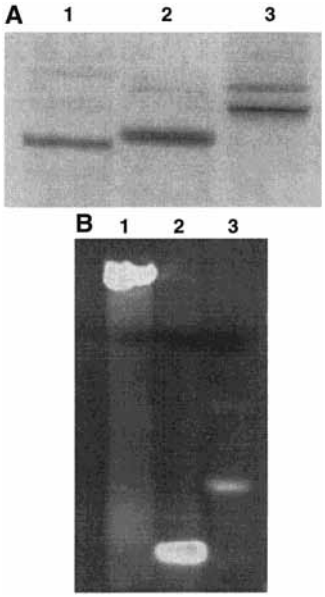

Figure 6. (A) Autoradiogram of a 20% denaturing polyacrylamide gel and of 5′-^{32}P-labeled **G3-D** (lane 1), **G3-H** (lane 2), and the **G3-H**/cisplatin reaction (lane 3). (B) EthBr staining of a 20% nondenaturing polyacrylamide gel of unlabeled **G3-D** (lane 1), **G3-H** (lane 2), and the **G3-H**/cisplatin reaction (lane 3).

^{31}P NMR Spectroscopy. Most of the ^{31}P NMR signals of **G3-H** appear in two clusters (−3.9 and −4.3 ppm, Supporting Information). An isolated signal, assigned to T_7pC_8 by a 2D selective reverse chemical shift experiment, has an upfield shift at −4.97 ppm, indicating that the backbone is distorted. With more added Zn^{2+} (or Mg^{2+}), the clusters merged and the −4.97 ppm signal decreased as a new signal appeared at −4.84 ppm. These results indicate slow interconversion of two forms. The less upfield shift of the −4.84 ppm signal suggests that the degree of backbone distortion is slightly smaller in **ZnG3-H** and **MgG3-H** vs **G3-H** and that the backbone distortion in the bulge is similar in both bulged duplexes.

***cis*-Pt(NH$_3$)$_2$Cl$_2$−G3-H Reaction in the Absence of M^{2+}.** Samples of **G3-D**, **G3-H**, and the reaction mixture between **G3-H** and *cis*-$Pt(NH_3)_2Cl_2$ were analyzed by 20% denaturing gel electrophoresis (Figure 6A). The *cis*-$Pt(NH_3)_2Cl_2$−**G3-H** reaction mixture (lane 3) contained faster and slower migrating products, referred to as Pt-1 and Pt-2, respectively. As quantitated by liquid scintillation, the Pt-1:Pt-2 ratio was ∼28:72, different from the 4:96 ratio found in the **G3-D** reaction.[37] Platination sites were determined by sequencing as previously described.[37] In Figure 7, untreated **G3-H** (lane 1), Pt-1 (lane 2), and Pt-2 (lane 3) were loaded onto the denaturing gel as controls. On treatment of Pt-1 and Pt-2 with NaCN (lanes 3 and 5, respectively) for 36 h, most of the platinum was removed, although a small amount of **G3-H** adduct remained. Bands of the DMS reaction indicated strand cleavage at all three G's, as expected for **G3-H** (lane 6). Strand cleavage was found at G_5 for Pt-1 (lane 7), indicating that Pt-1 has the G_3,G_4 cross-link, and at G_3 for Pt-2 (lane 8), indicating that Pt-2 has the G_4,G_5 cross-link. For the reaction of **G3-H** with $KMnO_4$, followed by hot alkali treatment (lane 10), the T_6 residue was found to be more reactive than T_7. This observation supports our conclusions based on NMR results that, in the hairpin conformation, T_6 is more exposed to solvent than T_7.

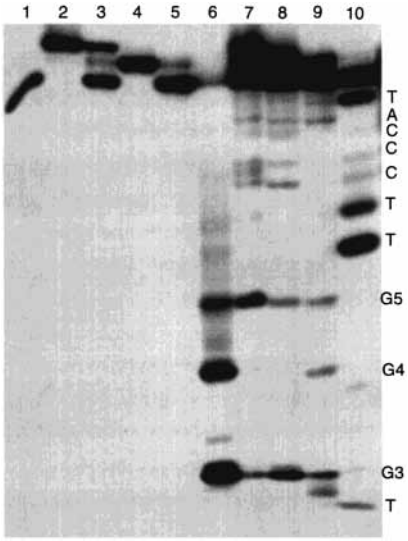

Figure 7. Autoradiogram of a 20% denaturing polyacrylamide gel of 5′-^{32}P-labeled **G3-H** (lane 1), Pt-1 (G_3,G_4, lane 2) and Pt-2 (G_4,G_5, lane 4) of **G3-H**, Pt-1 (G_3,G_4) and Pt-2 (G_4,G_5) following treatment with 0.1 M NaCN (lanes 3 and 5, respectively), DMS reaction with **G3-H** (lane 6), Pt-1 (G_3,G_4, lane 7), and Pt-2 (G_4,G_5, lane 8), reactions of **G3-H** with piperidine−formate (lane 9), and $KMnO_4$ (lane 10).

On the denaturing gel, both **G3-H** adducts have a mobility slower than that of **G3-D** (lane 1) and **G3-H** (lane 2) but similar to that of G_3,G_4 **G3-D** adduct. The G_4,G_5 **G3-D** adduct has a faster mobility (similar to free **G3-D**) than all of the previously mentioned adducts. On a nondenaturing gel, both **G3-H** adducts have exactly the same electrophoretic mobility, as assessed by both UV shadowing and ethidium bromide (EthBr) staining (Figure 6B, lane 3), a result suggesting that both have similar secondary structure under nondenaturing conditions.

In our past studies, we showed that assessment of the ratio of cross-linked adducts by the 5′-^{32}P-end labeling method may not be accurate. Although the minor **G3-D** adduct (G_3,G_4) was only ∼4% of the total product as found by UV-shadowing, the 5′-end labeling experiments made it appear to be a substantial portion of the total product.[37] The G_3,G_4 **G3-D** cross-linked adduct is more efficiently labeled using T4 polynucleotide kinase, due to the adduct's less favorable terminal base-pairing.[37] The G_4,G_5 **G3-D** adduct retained its hairpin form; this form has minimal end fraying and is thus not efficiently recognized by T4 polynucleotide kinase. For this reason, we analyzed G_3,G_4 and G_4,G_5 **G3-H** adducts by UV shadowing and EthBr staining (Figure 8). Figure 8 shows two pictures of the same denaturing gel with either 3 or 7 nmol of **G3-D** (lanes 3,6), **G3-H** (lanes 2,5), and the **G3-H**−*cis*-$Pt(NH_3)_2Cl_2$ reaction (lanes 1,4). The UV-shadowing analysis of the gel in Figure 8A indicates that the G_3,G_4 and G_4,G_5 **G3-H** adducts were present in the same ratio as found with the 5′-^{32}P-end labeling experiments. Thus, both products were labeled by the kinase with similar efficiency.

Some results suggest that the G_4,G_5 adducts may have less end-fraying under conditions of a denaturing gel. The G_4,G_5 **G3-H** band was stained well by EthBr (Figure 8B), but the G_3,G_4 **G3-H** band was not stained. Both the G_3,G_4− and G_4,G_5− **G3-D** bands are efficiently stained by EthBr (data not shown). The fluorescence of EthBr is proportional to the amount of double-stranded structure of the DNA present.[57] Thus, the G_4,G_5−**G3-H** and both **G3-D** adducts probably form hairpins under denaturing conditions, while the G_3,G_4−**G3-H** adduct does not. The G_3,G_4−**G3-D** adduct may also favor a hairpin conformation with A_7 tucked inside of the loop, similar to the G_4,G_5−**G3-D** adduct.[37] Differences in conformation may account for the slightly faster mobility of the G_4,G_5 adducts than the G_3,G_4 adducts in the denaturing gel. Both of the **G3-H** adducts and the G_3,G_4-**G3-D** adduct have single-stranded coil mobility and are stained under nondenaturing conditions, suggesting that all form weak hairpins.

***cis*-$Pt(NH_3)_2Cl_2$ Reaction with G3-H and G3-D in the Presence of M^{2+}.** To determine the effects on the G_3,G_4:G_4,G_5 adduct ratio due to the formation of a bulged duplex, *cis*-$Pt(NH_3)_2Cl_2$−**G3-H** reactions were performed in the presence of 4 mM or 20 mM $Mg(NO_3)_2$ and 5 mM $Zn(NO_3)_2$. Metal ion concentrations were chosen so as to provide conditions similar to the NMR experiments. Zn^{2+} changed the G_3,G_4:G_4,G_5 ratio only slightly to 33:67 (Figure 9, lane 4), but Mg^{2+} had no effect (lane 5). However, these reactions generally took 4−5 days for completion vs only 2 days in the absence of metal ions. Rates of the *cis*-$Pt(NH_3)_2Cl_2$−**G3-D** reactions were similar to those of the **G3-H** reactions in the presence and absence of M^{2+}. Addition of M^{2+} did not change the cross-linked product ratio (data not shown).

***cis*-$[Pt(NH_3)_2(H_2O)_2]^{2+}$ Reaction with G3-H and G3-D in the Presence and Absence of M^{2+}.** Reactions of **G3-H** and **G3-D** with *cis*-$[Pt(NH_3)_2(H_2O)_2]^{2+}$ were also examined to determine if the cross-linked adduct ratios depended on leaving ligand. The G_3,G_4:G_4,G_5 ratios in the *cis*-$[Pt(NH_3)_2(H_2O)_2]^{2+}$−**G3-H** reactions were the same as found in the *cis*-$Pt(NH_3)_2Cl_2$−**G3-H** reactions both in the absence and presence of Mg^{2+} and Zn^{2+} (data not shown). The G_3,G_4:G_4,G_5 ratio for the *cis*-$Pt(NH_3)_2Cl_2$−**G3-D** reaction (∼4:96) changed dramatically to ∼50:50 when *cis*-$[Pt(NH_3)_2(H_2O)_2]^{2+}$ was used (Figure 10B, lanes 5, 6). Chloride must affect the cross-linking step with **G3-D**. Addition of Zn^{2+} or Mg^{2+} to the *cis*-$[Pt(NH_3)_2(H_2O)_2]^{2+}$−**G3-D** reaction did not change the cross-linked adduct ratio of 50:50.

Previously, the G_4,G_5-**G3-D** adduct was demonstrated to be the cross-linked adduct by enzymatic hydrolysis and HPLC analysis of the products.[37] Above, the *cis*-$Pt(NH_3)_2Cl_2$:**G3-H** reaction ratio was 1:1. No free **G3-H** was found in the reaction, but two G's were platinated, providing strong evidence that Pt-1 and Pt-2 must be cross-linked products and not two Pt monoadducts of **G3-H** (2Pt/**G3-H**). Electrophoretic mobility is proportional to the net charge of the molecule and to the molecular mass.[58] Our finding that the related product of both *cis*-$[Pt(NH_3)_2(H_2O)_2]^{2+}$ and *cis*-$Pt(NH_3)_2Cl_2$ reactions with **G3-H** (and with **G3-D**) had the exact same mobility provides further evidence that the final products formed in all reactions have one cross-linked Pt moiety. The results discussed next confirm this conclusion.

Trapping of the G_4 Monoadduct with Dimethylthiourea (DMTU). Since a monoadduct must form as a precursor to the cross-linked adducts, DMTU was added to the reaction mixtures to determine if the monoadduct could be trapped. **G3-H** (Figure 10A) and **G3-D** (Figure 10B) were allowed to react with *cis*-$Pt(NH_3)_2Cl_2$ (20 μL total volume) for 2 days in deionized water (lanes 1, 2). The same reaction was also performed in 50 mM NaCl (lanes 3, 4) to slow the cross-linking step by decreasing Cl^- dissociation and with *cis*-$[Pt(NH_3)_2(H_2O)_2]^{2+}$ (lanes 5, 6) to accelerate the cross-linking step. After 2 days, each reaction solution was divided evenly into two Eppendorf tubes. DMTU

(57) Le Pecq, J.-B. In *Methods of Biochemical Analysis*; Glick, D., Ed.; John Wiley and Sons: New York, 1971; Vol. 20, pp 41−86.

(58) Offord, R. E. In *Methods In Enzymology*; Colowick, S. P., Kaplan, N. O., Eds.; Academic Press: New York, 1977; Vol. XLVII, pp 51−69.

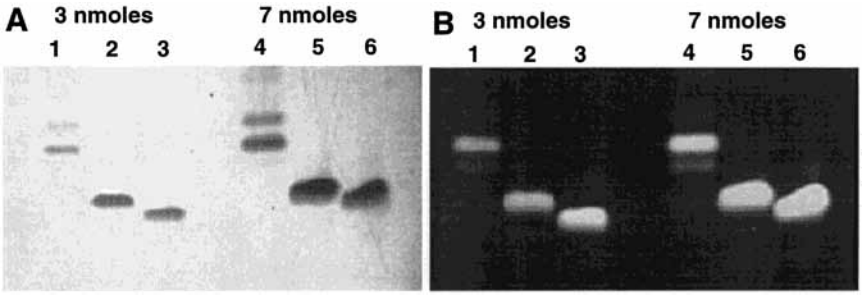

Figure 8. EthBr staining (A) and UV shadowing (B) analyses of a 20% denaturing polyacrylamide gel of 3 nmol (lanes 1−3) or 7 nmol (lanes 4−6) of **G3-H**/cisplatin (lanes 1, 4), **G3-H** (lanes 2, 5), and **G3-D** (lanes 3, 6).

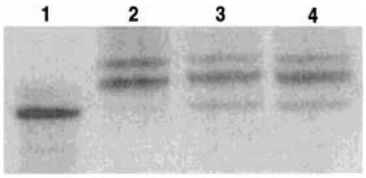

Figure 9. Autoradiogram of a 20% denaturing polyacrylamide gel of 5′-^{32}P-labeled **G3-H** (lane 1) and the reaction between cisplatin and **G3-H** with no metal cations (lane 2), 5 mM Zn^{2+} (lane 3), and 20 mM Mg^{2+} (lane 4).

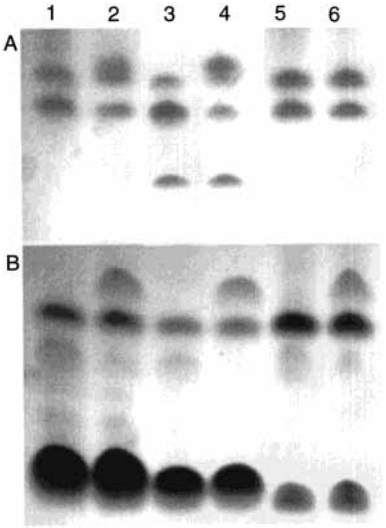

Figure 10. UV shadowing analysis of the reactions of **G3-H** (A) and **G3-D** (B) with *cis*-$Pt(NH_3)_2Cl_2$ (lanes 1−4) or *cis*-$[Pt(NH_3)_2(H_2O)_2]^{2+}$ (lanes 5, 6) with (even lanes) and without (odd lanes) DMTU added. Reactions were performed for 2 days in deionized H_2O (lanes 1, 2, 5, 6) or in 50 mM NaCl (lanes 3, 4).

(1 μL of 0.1 M DMTU) was added to one tube (even-numbered lanes). All solutions were frozen for ∼5 h before loading onto a denaturing gel. A new band indicating that a monoadduct was trapped with DMTU was observed in all reaction solutions except for that of *cis*-$[Pt(NH_3)_2(H_2O)_2]^{2+}$−**G3-H**. Migration of the new band was slower than that of the bands of the cross-linked adducts. There was no apparent difference in the relative amount of trapped monoadduct in the *cis*-$Pt(NH_3)_2Cl_2$−**G3-H** or −**G3-D** reactions in the presence or absence of 50 mM NaCl. While no free **G3-H** was detected in reactions without NaCl, some free **G3-H** remained in the 50 mM NaCl reaction with *cis*-$Pt(NH_3)_2Cl_2$ after 2 days (lanes 3, 4). No free **G3-D** was detected in the 50 mM NaCl reaction with *cis*-$Pt(NH_3)_2Cl_2$. This result suggests that the decreased amount of $[Pt(NH_3)_2(H_2O)Cl]^+$ slowed the rate of formation of the monoadduct of **G3-H**.

Treatment of the DMTU adduct with NaCN afforded free **G3-H** after only 20 h (lane 5, Figure 11). Even after 36 h of

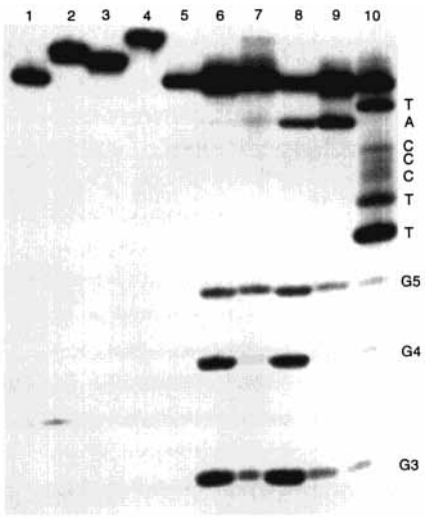

Figure 11. Autoradiogram of a 20% denaturing polyacrylamide gel of 5′-^{32}P-labeled DMTU-trapped cisplatin/**G3-H** and sequencing analysis. Lanes 1−4 contain **G3-H**, G_3,G_4, G_4,G_5, and the DMTU-trapped product of cisplatin/**G3-H**, respectively. Lane 5 contains the DMTU-trapped product after ∼20 h of treatment with 0.1 M NaCN at 37 °C. Also shown are the DMS reaction and hot alkali treatment with **G3-H** (lane 6), DMTU-trapped product (lane 7), and Maxam−Gilbert reactions of **G3-H** (G + A, lane 8; A, lane 9; T, lane 10).

NaCN treatment, the G_3,G_4 and G_4,G_5 adducts were only partially converted to free **G3-H**. DMS treatment of the new DMTU species showed a substantial amount of cleavage at G_3 and G_5 (lane 7, Figure 11), indicating that the new product is the G_4 monoadduct of **G3-H**. The DMTU-trapped adduct of **G3-D** was also the G_4 monoadduct (data not shown) in both the *cis*-$Pt(NH_3)_2Cl_2$ and *cis*-$[Pt(NH_3)_2(H_2O)_2]^{2+}$ reactions. The G_4 adduct was formed almost exclusively in the reactions of **G3-D** with $[Pt(dien)Cl]^+$ (dien = diethylenetriamine).[37] Likewise, we observed that $[Pt(dien)Cl]^+$ adds to this site in **G3-H** (data not shown). Trapping of only the G_4 monoadducts for both **G3-H** and **G3-D** provides more evidence that the G_3,G_4 and G_4,G_5 adducts are cross-linked products.

It has been shown that 10 mM thiourea can strip platinum from cellular DNA when incubated at 37 °C for several hours.[59] To determine whether the **G3-H** cross-linked adducts were being stripped or partially stripped of platinum by DMTU, the cross-linked adducts were eluted from the gel and ethanol precipitated. Purified cross-linked adducts were incubated in 10 mM DMTU for various lengths of time at various temperatures. The cross-linked products were stable in 10 mM DMTU, even after heating at 37 °C for 48 h (Supporting Information). Under the isolation

(59) Fichtinger-Schepman, A. M. J.; van Dijk-Knijnenburg, H. C. M.; Dijt, F. J.; van der Velde-Visser, S. D.; Berends, F.; Baan, R. A. *J. Inorg. Biochem.* **1995**, *58*, 177−191.

Scheme 3. General Schematic Representation of Conformers of **G3-H** Induced by Various Metal Ions and Cisplatin[a]

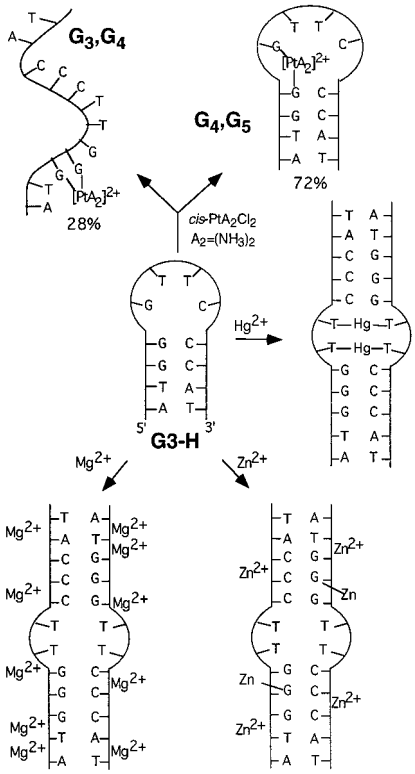

[a] Predicted conformers of cisplatin-**G3-H** adducts under denaturing conditions.

conditions for the G_4 monoadduct, we found no stripping of platinum from the cross-linked adducts by DMTU. Because it can capture the monoadduct without stripping the cross-linked adducts, DMTU is useful in studying monoadduct formation in these oligonucleotides.

Discussion

Scheme 3 depicts the various interactions of metal species with **G3-H** and the resulting forms of the adducts. Except for interactions of Hg^{2+} which produced the bulged duplex form of **G3-H** with two interstrand T−Hg^{2+}−T cross-links described previously,[8] all of the other results depicted in Scheme 3 are from the current study and are discussed below.

Features of G3-H. The imino ^{1}H NMR signals provide useful information on the conformation of the hairpin form of free **G3-H**. For typical duplexes, the imino signal for the terminal base pair is often not observed,[30,60,61] but this signal is often observed for hairpin forms.[62,63] Observation of the terminal T_{12}N(3)H signal at room temperature (Supporting Information) is consistent with a hairpin form, but the signal is upfield and broad, indicating end fraying. The slight broadening of the T_2N(3)H signal indicates that some end fraying extends to this base pair. Even the G_3N(1)H signal was relatively less sharp than the G_4N(1)H signal. Taken together, these results suggest that cooperative end fraying may occur.

The G_4N(1)H signal was the sharpest peak at 12 °C and shifted only slightly upfield at 23 °C. However, the signal was broad compared to **G3-D**. For most other hairpins studied thus far with a GC base pair in the stem nearest the loop region, the imino signals have chemical shifts of ∼12.6−12.9 ppm.[61,63−65] Our results for the hairpin form of **G3-H** are consistent with such findings and indicate that a stable G_4C_9 base pair is present. No clearly base-paired imino signal was observed for G_5N(1)H at any temperature. A broad signal at ∼11.6 ppm was most readily observed at ∼25−30 °C. The chemical shift of the imino signal of G varies greatly when it is not in a Watson−Crick (WC) base pair.[65,66] The 11.6 ppm signal observed here is consistent with a protected, weakly H-bonded G_5N(1)H. An inter-base-pair G_4N(1)H−G_3N(1)H NOE was found, but no such NOE for the G_5N(1)H signal was detected. These results suggest that the stacking between G_3C_{10} and G_4C_9 base pairs is normal, but stacking between the G_4C_9 base pair and the G_5 and C_8 residues is not normal. The NOE pattern suggests that G_4−G_5 base stacking is weak, a finding different from those for other hairpins.[63,64]

Imino protons that are enclosed in a hydrophobic or protected region even in the absence of WC base pairing have observable signals because the proton exchange rate is slow.[63,66] It has been suggested that these regions are hydrophobic as a result of base stacking.[63] Indeed, we observed the T_6N(3)H and T_7N(3)H signals of **G3-H** in the hairpin and in the bulged duplex forms. These signals were observed between 10.7 and 10.9 ppm, indicating the absence of WC base pairing. The two signals for the hairpin had the same intensity and broadened simultaneously, suggesting a similar solvent accessibility to the two imino protons.

For the hairpin form, the absence of NOEs between the T_6N(3)H and T_7N(3)H signals and weak or absent T_6H6−T_7CH_3 and T_6H1′−T_7H6 NOE cross-peaks (Supporting Information) indicate weak, if any, stacking interaction between T_6 and T_7. However, G_5−T_6 stacking is likely since the G_5H8−T_6CH_3 and the G_5H1′−T_6H2′/2″ NOE cross-peaks (Supporting Information) were observed. Very weak T_7H6−C_8H5, T_7H2′−C_8H6, and T_7H1′−C_8H6 NOE cross-peaks and the unusual G_5H8−T_7CH_3 NOE cross-peak all suggest weak stacking between T_7 and C_8. Moreover, T_7 is positioned close to G_5 and is probably located toward the inside of the loop, a conformation requiring that the backbone be distorted at T_7. The sharp upfield T_7pC_8 ^{31}P NMR signal supports this conclusion. The absence of a C_8H6−C_9H5 NOE cross-peak suggests a poor stacking interaction between C_8 and C_9.

In the D_2O spectra of the hairpin form, the intraresidue base proton−H1′ NOE cross-peaks of the stem region were weaker than the cytidine H5/H6 cross-peaks (Supporting Information), indicating that all residues have an anti-conformation. The NOE cross-peaks observed between a base proton and its own H1′ and also the 5′-adjacent H1′ (particularly the A_1H8−T_2CH_3 and A_{11}H8−$T_{12}CH_3$ NOE cross-peaks) indicate that the stem is in a right-handed helical form. Most of the shifts of the ^{13}C signals for both sugars and bases in the stem region of the hairpin form of **G3-H** were normal compared with those of **G3-D** (Table 2 and Supporting Information).

Previous Studies of Zn^{2+} Addition to G3-D. Although **G3-D** was found to be mostly a stable duplex, some hairpin

(60) Kouchakdijk, M.; Li, B. F. L.; Swann, P. F.; Patel, D. J. *J. Mol. Biol.* **1988**, *202*, 139−155.
(61) Rajagopal, R.; Gilbert, D. E.; van der Marel, G. A.; van Boom, J. H.; Feigon, J. *J. Magn. Reson.* **1988**, *78*, 526−637.
(62) Haasnoot, C. A. G.; de Bruin, S. H.; Berendsen, R. G.; Janssen, H. G. J. M.; Binnendijk, T. J. J.; Hilbers, C. W.; van der Marel, G. A.; van Boom, J. H. *J. Biomol. Struct. Dyn.* **1983**, *1*, 115−129.
(63) Hare, D. R.; Reid, B. R. *Biochemistry* **1986**, *25*, 5341−5350.
(64) Wemmer, D. E.; Chou, S. H.; Hare, D. R.; Reid, B. R. *Nucleic Acids Res.* **1985**, *13*, 235−246.
(65) Patel, D. J.; Koslowski, S. A.; Ikuta, S.; Itakuta, K. *Biochemistry* **1984**, *23*, 3207−3217.
(66) Gupta, G.; Sarma, M. H.; Sarma, R. H. *Biochemistry* **1987**, *26*, 7715−7723.

form was evident.[30] Addition of Zn^{2+} stabilized the duplex form and eliminated the **G3-D** hairpin form.[30] Chemical shifts were affected by Zn^{2+} (Tables 1 and 2 and Supporting Information), especially for the G_4H8 and G_4C8 signals, due to Zn^{2+} binding to G_4N7.[30] No significant changes in the relative intensities of the NOE cross-peaks of the **G3-D** duplex upon addition of Zn^{2+} were observed, suggesting that no large conformational changes of the duplex occurred.[30]

Bulged Duplex Conformation. The G_4H8 signal shifted downfield upon initial addition of Zn^{2+} to **G3-H**, indicating that Zn^{2+} binds to G_4N7 of the **G3-H** hairpin. The **G3-H** hairpin was converted to a C_2-symmetrical "self-complementary" bulged duplex form upon further addition of Zn^{2+} or with Mg^{2+} addition. Both metal ions influenced the signals of the three terminal base pairs. On Zn^{2+} addition, the two AT base pair imino signals shifted downfield and sharpened only slightly (Supporting Information). This result suggests that Zn^{2+} has relatively little effect on the end fraying. In contrast, the sharpening of the $G_3N(1)H$ signal caused by Zn^{2+} was accompanied by a downfield shift to 13.3 ppm. However, for **MgG3-H**, this signal was also at ~13.3 ppm but was broader than the $T_2N(3)H$ signal. The $T_2N(3)H$ and the $T_{12}N(3)H$ signals were sharper and further downfield for **MgG3-H** than for the hairpin or for **ZnG3-H**. Thus, it appears that Mg^{2+} is effective at stabilizing the AT ends, whereas Zn^{2+} preferentially stabilizes the GC region. For **G3-D**, the metal ions also appeared to stabilize the duplex form and decrease end-fraying under most conditions.[30]

Typical NOE intra- and interresidue cross-peaks were observed for the signals of H1′ and the base protons of **G3-H** for the stem regions of **ZnG3-H**. In agreement with Wemmer's analysis,[64] the $A_1H1'-T_2H6$ and $A_{11}H1'-T_{12}H6$ NOE cross-peaks were stronger than those for $T_2H1'-G_3H8$ and $C_{10}H1'-A_{11}H8$, which in turn were stronger than the corresponding NOE cross-peaks for the hairpin form. $A_1H8-T_2CH_3$ and $A_{11}H8-T_{12}CH_3$ NOE cross-peaks with moderate intensities were also found. Similar results were found for **MgG3-H**, although overlap obscured some cross-peaks. These results indicate that the terminal regions ($A_1T_2G_3{\cdot}C_{10}A_{11}T_{12}$) in the bulged duplexes adopt a more normal right-handed helical conformation than in the hairpin form. Indeed, most of the shifts of the ^{13}C signals for both sugars and bases in the two bulged duplex forms are normal relative to those of **G3-D** (Table 2 and Supporting Information). The ~1.5 ppm further upfield shift for the $T_{12}C4'$ (85.0 ppm) signal of **MgG3-H** compared to other forms (86.5 ppm in **G3-D**) may reflect some slight conformational changes at the terminal base pair, as also suggested by the ^1H NMR signals of **MgG3-H**.

Signals for the region between the terminal base pairs and the bulge and for the bulge region are more interesting. The $G_4N(1)H$ signal of **ZnG3-H** is relatively downfield at 13.25 ppm (Figure 3) because Zn^{2+} binds to G_4N7 (see below). This signal did not shift with increasing temperature and was sharper than the $G_4N(1)H$ signal of the hairpin form at 30 °C. However, for both forms, the signal was severely broadened at 35 °C. These results suggest that the G_4C_9 base pair is stabilized only slightly compared to the hairpin form. The $G_5N(1)H$ signal of **ZnG3-H** was sharp and clearly had the intensity of one proton, consistent with a stable G_5C_8 base pair. With an increase in temperature, the broadening was similar to that of the other GC imino signals, suggesting that the nearby bulge has little effect on the stability of the G_5C_8 WC base pair. Inter-base-pair imino proton NOEs were found for $G_4N(1)H-G_5N(1)H$ and for $G_3N(1)H-G_4N(1)H$. A strong C_8H6-C_9H5 NOE cross-peak was also observed. In addition, the observed $G_5H8-T_6CH_3$ NOE cross-peak indicated G_5-T_6 base stacking. However, the absence of the normally observed $G_5H8-G_4H2'/2''$ and $T_6H6-G_5H2'/2''$ NOE cross-peaks suggests that the G_5 residue of **MZnG3-H** is not completely in a normal position for B-DNA.

For **MgG3-H** at 12 °C, the observed inter-base-pair $G_4N(1)H-G_3N(1)H$ and $G_4N(1)H-G_5N(1)H$ NOEs and the narrow widths of the signals suggest strong base stacking in the GC region of **MgG3-H**. The shift of the $G_4N(1)H$ signal was only ~0.1 ppm downfield compared to **G3-H**, but ~0.2 ppm upfield compared to **ZnG3-H**. The $G_5N(1)H$ signal at ~12.9 ppm was also ~0.2 ppm upfield compared to that of **ZnG3-H**. The differences in shift between **ZnG3-H** and **MgG3-H** are attributable to the absence of GN7 binding of Mg^{2+}. The two GN(1)H signals of **MgG3-H** were sharp even at 35 °C (Figure 5). In contrast, at 35 °C the two signals of **ZnG3-H** and the $G_4N(1)H$ signal of **G3-H** were extremely broad (Figure 4). These results suggest that G_4C_9 and G_5C_8 base pairing is significantly more favored in **MgG3-H** at higher temperature. As we proposed in a study of the effects of Zn^{2+} on DNA polymers,[20] we believe that the interaction with cytidine N3 by Zn^{2+} disrupts base pairing and accounts for these results.

Other differences were found between the hairpin and the bulged duplex forms. For **ZnG3-H**, in contrast to the hairpin, weak stacking between T_6 and T_7 is suggested by the weak $T_6H6-T_7CH_3$ and $T_6H1'-T_7CH_3$ NOE cross-peaks. Some normally observed NOE cross-peaks ($G_5H8-G_4H2'/2''$ and $T_6H6-G_5H2'/2''$) were missing, indicating that G_5 is not in a normal helix position. However, the strong $G_5H8-T_6CH_3$ and $G_5H1'-T_6CH_3$ NOE cross-peaks suggest that there is base stacking with the $G_5-T_6-T_7$ segment but that T_6 and T_7 are not positioned as in a normal duplex. We attribute this effect to the distortion caused by Zn^{2+} binding at G_4N7 (Scheme 3). In addition, the absence of $T_6N(3)H-T_7N(3)H$ or $T_6N(3)H-G_5N(1)H$ NOEs suggests that a wobble T·T mismatched base pair is not present.[60]

It is likely that the sugar ^{13}C shifts reflect the backbone conformation. Several sugar ^{13}C signals of G_5, T_6, T_7, C_8, and C_9 were shifted upfield (~1.3−4.2 ppm) upon addition of Zn^{2+} and Mg^{2+} (Table 2). These upfield shifts are obviously due to the conformational change of the strand from the hairpin to the duplex form, since the shifts of many of these signals are similar to those of the corresponding signals of the **G3-D** duplex. These similarities suggest that the transition from the hairpin to the bulged duplex form converts the backbone toward a more normal duplex structure. However, significant differences in chemical shifts between the bulged duplexes and **G3-D** were still evident for several signals. These differences indicate the presence of a bulge and slight distortions of the backbone in the central region, in agreement with observations from the ^1H and ^{31}P NMR spectra.

The chemical shifts of base carbons were found to be very sensitive to metal ion binding. For example, the G_4C8 signal shifted downfield ~1.7 ppm due to Zn^{2+} binding at G_4N7 (Table 2). Mg^{2+} did not shift this signal significantly, consistent with the conclusion above that Mg^{2+} did not bind to bases (Scheme 3). This observation agrees with the previous finding that Zn^{2+} binding to GN7 resulted in a ~2 ppm downfield shift of the C8 signal.[67]

The chemical shifts of the C_8 C1′, C3′, and C4′ signals for **ZnG3-H** were closer to those of **G3-D** than those for **MgG3-H**, suggesting that the C_8 residue is in a more normal position

(67) Marzilli, L. G.; deCastro, B.; Solorzano, C. *J. Am. Chem. Soc.* **1982**, *104*, 461−466.

in **ZnG3-H** than in **MgG3-H**. In contrast, the shifts of the T_6 sugar signals of **MgG3-H** are closer to those of **G3-D** than those of **ZnG3-H**, suggesting that the T_6 residue is in a more normal duplex position in **MgG3-H** than in **ZnG3-H**. These data reflect the advantage of using ^{13}C NMR spectroscopy since this region could not be observed clearly from ^1H NMR spectra due to NOE cross-peak overlap. Most importantly, the results suggest that *binding of a base nitrogen in a monoadduct can influence the conformation of nearby residues.*

Addition of Hg^{2+} to **G3-H** has also been shown to result in the formation of a bulged duplex.[8] Despite the differences between DNA binding preferences of Zn^{2+}, Mg^{2+}, and Hg^{2+}, these divalent metal cations all induced a bulged duplex form of **G3-H** (Scheme 3). Only Zn^{2+} binds to a base site in the major groove (GN7), although it appears to bind only as a monoadduct.

Monoadducts Involving G3-H and G3-D with Pt Compounds. Monoadducts are important since these are precursors in the cross-linking process by Pt anticancer drugs. Unlike the case of Zn^{2+}, where binding sites are thermodynamically controlled, Pt(II) reaction sites are kinetically controlled. Therefore, the initial binding step is crucial in determining which DNA segment forms an adduct. For **G3-D**, G_4N7 and G_3N7 are the first and second most nucleophilic sites according to electrostatic potential calculations and the determination of metal binding sites by NMR methods and sequencing analysis.[30,37] These sites are also most reactive toward Zn^{2+} for **G3-H**. The G_4 adduct was formed almost exclusively in the reactions of **G3-D** and **G3-H** with $[Pt(dien)Cl]^+$.[37] Therefore, the detection of only the G_4-monoadduct of both **G3-D** and **G3-H** (Figure 11) for *cis*-$Pt(NH_3)_2Cl_2$ is the expected result. However, the intermediacy of minor amounts of G_3 or G_5 monoadducts that form cross-links too quickly for trapping by DMTU cannot be ruled out for either oligonucleotide.

In the *cis*-$Pt(NH_3)_2Cl_2$ reactions, the reactive *cis*-$[Pt(NH_3)_2(H_2O)Cl]^+$ cation initially adds to **G3-D** or **G3-H** to form primarily the Cl−G_4 monoadduct. In the *cis*-$[Pt(NH_3)_2(H_2O)_2]^{2+}$ reactions, only the H_2O−G_4 monoadduct is formed. Because the G_4 monoadduct was trapped in the *cis*-$[Pt(NH_3)_2(H_2O)_2]^{2+}$ and *cis*-$Pt(NH_3)_2Cl_2$ reactions with **G3-D** (Figure 10), both the Cl− and H_2O−G_4 monoadducts of **G3-D** are relatively long-lived. The Cl−G_4 monoadduct of **G3-H** was also trapped with DMTU. However, no monoadduct was found in the reaction *cis*-$[Pt(NH_3)_2(H_2O)_2]^{2+}$ with **G3-H**, suggesting that the H_2O−G_4 monoadduct of **G3-H** forms cross-linked adducts quickly. Thus, any H_2O−G_4 monoadduct trapped by DMTU would be below the detection limit. Before discussing the relationship of the monoadducts to the cross-linking process, we shall briefly review previous reports on cross-linking by monoadducts.

Past Studies of Oligonucleotides with *cis*-$[Pt(NH_3)_2(H_2O)_2]^{2+}$ and *cis*-$Pt(NH_3)_2Cl_2$. From kinetic studies of platination of single-stranded[68] and double-stranded[69] GpG-containing oligonucleotides by *cis*-$[Pt(NH_3)_2(H_2O)_2]^{2+}$, Chottard et al. found that 5′-chelation was ∼13 times faster than 3′-chelation; they attributed this effect to a more nucleophilic 5′-G than 3′-G in their sequence and to the helical arrangement of the DNA such that the 5′-G is closer to the platinum in the 3′-G monoadduct.[69] However, in energy-minimized molecular models of $Pt(NH_3)_3$−G and −A adducts in GAGG/CCTC and GGAG/CTCC duplexes, the purines that were 3′ and 5′ to the platinated G or A were relatively equidistant from Pt.[70] A recent study of a 20-nucleotide hairpin having two consecutive G's revealed that, although both G's formed a monoadduct with *cis*-$[Pt(NH_3)_2(H_2O)_2]^{2+}$ at similar rates, 5′-chelation was ∼10 times faster than 3′-chelation.[71] After the initial binding of *cis*-$Pt(NH_3)_2Cl_2$ to G_4 of **G3-D**, chelation to G_5 occurred almost exclusively in the 3′-direction, forming the major G_4,G_5 adduct.[36,37] Even though 5′-chelation is usually favored[68,69] and the 5′-G (G_3) is more nucleophilic than the 3′−G (G_5) in **G3-D**,[30,37] the 3′-cross-linked product formed preferentially.

Scheme 4

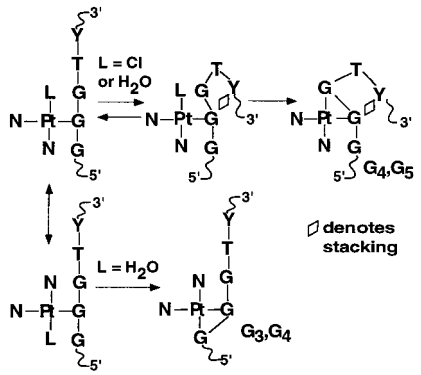

Reaction of G3-D with *cis*-$Pt(NH_3)_2Cl_2$ vs *cis*-$[Pt(NH_3)_2(H_2O)_2]^{2+}$. From the G_3,G_4:G_4,G_5 product ratio found for the different reactions reported here, it is clear that the reaction of **G3-D** with *cis*-$Pt(NH_3)_2Cl_2$ (∼4:96) is remarkably specific. The Cl−G_4 monoadduct may induce a population of a distorted form having G_5 positioned to form a bond to Pt, possibly because of stacking of G_4 with A_7. Cross-linking then occurs quickly and primarily in the 3′-direction before hydrolysis to the H_2O−G_4 monoadduct can occur (Scheme 4). The 50:50 cross-linked product ratio in the reaction of **G3-D** with *cis*-$[Pt(NH_3)_2(H_2O)_2]^{2+}$ suggests that the H_2O−G_4 monoadduct forms the cross-linked adducts mostly before conformational changes can occur. Other differences between the Cl− and H_2O−G_4 monoadducts of **G3-D** could lower the cross-linking selectivity. First, steric and/or hydrogen-bonding interactions might affect the relative orientations in the monoadduct forms. In Scheme 4, we show that two rotamers are possible for a monoadduct. The leaving ligand, L, will influence which rotamer is favored. The relative rates of 3′- and 5′- chelation are probably different for the two rotamers since L is in a different position in each rotamer. Second, the higher charge of the aqua adduct may disfavor the distorted form. Finally, as mentioned above, a reactive minor H_2O−G_3 monoadduct may form and this adduct can readily cross-link only with G_4.

Reaction of G3-H with *cis*-$Pt(NH_3)_2Cl_2$ and *cis*-$[Pt(NH_3)_2(H_2O)_2]^{2+}$ in the Absence and Presence of M^{2+}. The G_3,G_4:G_4,G_5 ratio was insensitive to the differences between the **G3-H** hairpin and the **ZnG3-H** and **MgG3-H** duplexes (Figures 6 and 9). Moreover, no dependence of this ratio on L was found for *cis*-$Pt(NH_3)_2Cl_2$ vs *cis*-$[Pt(NH_3)_2(H_2O)_2]^{2+}$. Chelation to the 3′-G (G_5) was favored over chelation to the 5′-G (G_3) in all forms of **G3-H**. Thus, as for **G3-D**, the cross-linking direction of **G3-H** is also different from that normally found.[68,69] In both the bulged duplex and the hairpin forms, G_5 is either near the bulged region or in the loop, whereas G_3 remains base-paired. Because G_5 is probably more fluxional than G_3, the G_4 monoadducts of **G3-H**

(68) Gonnet, F.; Reeder, F.; Kozelka, J.; Chottard, J.-C. *Inorg. Chem.* **1996**, *35*, 1653−1658.
(69) Reeder, F.; Gonnet, F.; Kozelka, J.; Chottard, J.-C. *Chem. Eur. J.* **1996**, *2*, 1068−1076.
(70) Hambley, T. *Inorg. Chem.* **1991**, *30*, 937−942.
(71) Legendre, F.; Kozelka, J.; Chottard, J.-C. *Inorg. Chem.* **1998**, *37*, 3964−3967.

favor 3′-chelation to G_5. These data for **G3-H** and **G3-D** all suggest that the local features of the GGG site strongly influence the cross-linking reaction, favoring 3′-chelation.

Conclusions

Several different Pt complexes and the Zn^{2+} cation selectively coordinate to N7 of the central G of the GGG sequence within a variety of conformational environments. Furthermore, the Pt monoadducts in every case undergo a high level of 3′-chelation, compared to the level normally expected. The very high preference for the formation of the G_4,G_5 cross-link over the G_3,G_4 cross-link in the cisplatin−**G3-D** reaction seems to be attributable to incipient formation of a hairpin form, which places G_5 in a favorable position to bind to Pt. The abnormally high ratio of G_4,G_5 to G_3,G_4 for **G3-H** suggests that flexibility in both the hairpin and the bulged duplex forms allows favorable binding by G_5. These results are of further interest because the dGGGT sequence is part of the repeat sequence in telomeres, which are believed to exhibit conformational diversity.

We have demonstrated the relationship between the properties of the metal center and the overall form and conformation of an oligonucleotide model. Several labile metal ions with different binding preferences have been shown to convert a hairpin form to a duplex form. On the other hand, Pt anticancer drugs appear to favor the hairpin form and convert a duplex into a hairpin form. EthBr staining analysis indicated that, under the conditions of the denaturing gel, the G_4,G_5 cross-linked **G3-H** adduct retained a weak hairpin conformation and the G_3,G_4 cross-linked **G3-H** adduct did not. The G_3,G_4 **G3-D** adduct also was a weak hairpin. Only the G_4,G_5 **G3-D** product seemed to favor highly the hairpin form, which is stabilized by stacking between G_5 and A_7. We conclude that the stability of the hairpin depends both on the position of the cross-link and on the sequence, with the substitution of just one base for another having a substantial effect on the stability. Other DNA sequences may also adopt unusual conformations when cross-linked by cisplatin. The conformations of the resulting adducts could be crucial to protein recognition and subsequent anticancer activity, repair, or mutagenesis. Changes in the carrier ligand may alter the product distribution and the final form of the adducts. We are now evaluating the effect of the carrier ligands in order to determine if such different conformers may explain the poor activity of cisplatin analogues.

Acknowledgment. This work was supported by NIH Grant GM 29222 (L.G.M.) and NIH Grant CA 73041 (National Cancer Institute) (P.W.D.).

Supporting Information Available: Full tables of ^{1}H and ^{13}C NMR chemical shift assignments, ^{1}H−^{13}C HMQC 2D NMR spectra, ^{1}H−^{1}H NOESY 2D NMR spectra, ^{1}H and ^{31}P 1D NMR spectra, and a UV-shadowed gel figure (DMTU with G_3,G_4 and G_4,G_5 **G3-H**). This material is available free of charge via the Internet at http://pubs.acs.org.

IC990603F